Hyperfine Structure

The nucleus has spin which is denoted by the quantum number I, which takes on integer or half-integer values

$$\vec{I}\cdot\vec{I} = I(I+1)\hbar^2$$
$$I_z = m_I \hbar$$

For the proton $I = \frac{1}{2}$, $I_z = \pm\frac{1}{2}\hbar$, $m_I = \pm\frac{1}{2}$

The nucleus has magnetic moment $\vec{\mu}_N = g_N \frac{e}{2Mc} \vec{I}$ where

M is the mass of the nucleus.
For the proton $g_N = 5.5855$

$$\vec{\mu}_p = 5.5855 \frac{e}{2Mc} \vec{I}$$

Interaction between the spin of the nucleus and the angular momentum of the electrons causes "hyperfine splitting", which is approximately (m_e/m_p) time smaller than fine-structure, or spin-orbit splitting.

The nuclear spin angular momentum can be added to the total electron angular momentum to give a new total angular momentum vector $\vec{F}$

$$\vec{F} = \vec{L} + \vec{S} + \vec{I} = \vec{J} + \vec{I}$$

$$\vec{F}\cdot\vec{F} = F(F+1)\hbar^2$$

The total angular momentum quantum number F can take on integrally spaced values between $|J-I|$ and $(J+I)$.

Example: Hydrogen ground state is $^2S_{1/2}$ $(J=\frac{1}{2})$
Proton spin $I = \frac{1}{2}$
$F = 0$ and 1

$\uparrow\downarrow$ $F=0$ $\quad$ $\uparrow\uparrow$ $F=1$

$\Delta E_1 - \Delta E_0 = \Delta E_{01} = 9.412 \times 10^{-18}$ erg
$= 1420 \times 10^6$ Hz
$A_{10} = 2.85 \times 10^{-15}\ s^{-1}$

Comparison of fine structure and hyperfine structure

The energy perturbation in fine-structure splitting of a hydrogenic atom is

Fine structure:
$$\Delta E_{fs} = \alpha^2 \frac{hcRZ^4}{n^3}\left[\frac{J(J+1) - L(L+1) - S(S+1)}{L(L+1)(2L+1)}\right]$$

where $\alpha = \frac{e^2}{\hbar c} = \frac{1}{137.0}$ is the "fine-structure constant"

$R = \frac{2\pi^2 \mu e^4}{ch^3}$ is the Rydberg constant $109737.312\ cm^{-1}$

$\mu = \frac{m_e M}{m_e + M}$ is the reduced mass

n is the principal quantum #

Z is the nuclear charge

Since the energy of the principal states of the hydrogenic atom are

$$E_n = -\frac{hcRZ^2}{n^2},$$

the fine-structure splitting $\Delta E_{fs} \approx \frac{\alpha^2 Z^2}{n} E_n \approx 10^{-4} E_n$

In contrast, the hyperfine splittings of hydrogenic atoms is

hyperfine structure:
$$\Delta E_{hfs} = 2 g_N \left(\frac{m_e}{m_p}\right) \frac{\alpha^2 hcRZ^3}{n^3}\left[\frac{F(F+1) - I(I+1) - J(J+1)}{J(J+1)(2J+1)}\right]$$

$$\Delta E_{hfs} \approx \left(\frac{m_e}{m_p}\right) \frac{\alpha^2 Z}{n} E_n \approx 10^{-7} E_n$$

Zeeman Effect - normal, when $S = 0$

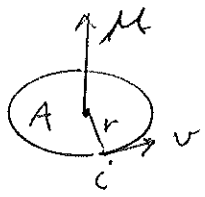

Consider the orbiting electron
To be a current loop.
The magnetic moment $\mu = \frac{iA}{c}$

The direction of μ is $q\vec{r}\times\vec{v}$

Current $i = -e\frac{v}{2\pi r}$

So $\mu = -\frac{ev}{2\pi rc}\pi r^2 = -\frac{1}{2}\frac{evr}{c}$

But $\vec{L} = m\vec{r}\times\vec{v}$ so $\boxed{\vec{\mu} = -\frac{e}{2mc}\vec{L}}$

Now apply an external magnetic field. The energy (potential) of a magnetic dipole in a magnetic field is

$\boxed{\Delta E = -\vec{\mu}\cdot\vec{B}}$

Let the direction z be defined as the direction of B. Then

$$\Delta E = +\frac{e}{2mc}L_z B = +\frac{e}{2mc}m_\ell \hbar B$$

(m_ℓ ← magnetic quantum number)

or $\Delta E = +m_\ell \mu_B B$ where $\mu_B = \frac{e\hbar}{2mc} = 9.27\times10^{-21}$ ergs/G

is the Bohr magneton

The "normal" Zeeman effect should produce an odd number of level splittings evenly spaced in energy.

Because the selection rules for allowed transitions between levels of different terms are $\Delta m_\ell = 0, \pm 1$ (but $m_\ell = 0 \not\leftrightarrow m_\ell = 0$), the line will be split into three components.

absorption

$$\Delta m_\ell = +1 \quad \nu = \nu_0 + \frac{eB}{4\pi mc} \quad \sigma_- \text{ component} \quad \text{(smaller wavelength)}$$

$$0 \quad \nu = \nu_0 \quad \pi \text{ component}$$

$$-1 \quad \nu = \nu_0 - \frac{eB}{4\pi mc} \quad \sigma_+ \text{ component} \quad \text{(larger wavelength)}$$

The π component is linearly polarized parallel to the magnetic field, while the σ components are elliptically polarized in opposite directions. In the direction of the magnetic field the π component vanishes, and the σ components are circularly polarized σ_+ (left), σ_- (right). In a direction perpendicular to the magnetic field, the σ components are linearly polarized perpendicular to the field

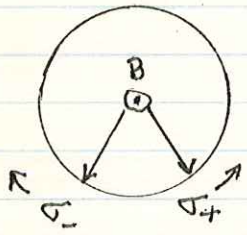

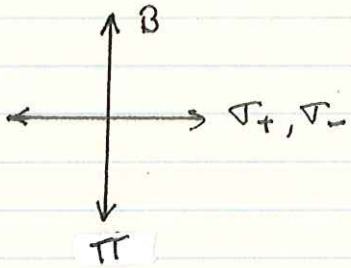

The frequency splitting between the components is

$$\Delta\nu_0 = \frac{eB}{4\pi mc} = 1.40 \times 10^6 \; B \; \text{Hz}$$

or $$\Delta\lambda_0 = \frac{c}{\nu_0^2}\Delta\nu_0 = \frac{\lambda_0^2}{c}\Delta\nu_0 = 1.16 \times 10^{-5} \left(\frac{\lambda_0}{5000\,\text{Å}}\right)^2 B \; \text{Å}$$

This can be much smaller than the intrinsic line width in the visible part of the spectrum, but magnetic fields in the sun and stars can be measured using circular polarimeters and seeing a shift in polarization in the wings of the line.

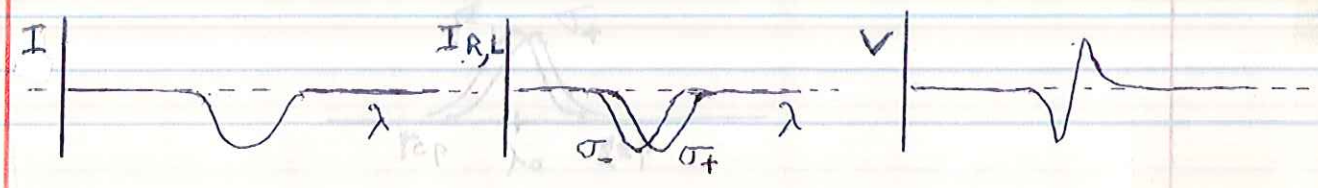

183

LETTERS

An 84-μG magnetic field in a galaxy at redshift $z = 0.692$

Arthur M. Wolfe[1], Regina A. Jorgenson[1], Timothy Robishaw[2], Carl Heiles[2] & Jason X. Prochaska[3]

The magnetic field pervading our Galaxy is a crucial constituent of the interstellar medium: it mediates the dynamics of interstellar clouds, the energy density of cosmic rays, and the formation of stars[1]. The field associated with ionized interstellar gas has been determined through observations of pulsars in our Galaxy. Radio-frequency measurements of pulse dispersion and the rotation of the plane of linear polarization, that is, Faraday rotation, yield an average value for the magnetic field of $B \approx 3\,\mu$G (ref. 2). The possible detection of Faraday rotation of linearly polarized photons emitted by high-redshift quasars[3] suggests similar magnetic fields are present in foreground galaxies with redshifts $z > 1$. As Faraday rotation alone, however, determines neither the magnitude nor the redshift of the magnetic field, the strength of galactic magnetic fields at redshifts $z > 0$ remains uncertain. Here we report a measurement of a magnetic field of $B \approx 84\,\mu$G in a galaxy at $z = 0.692$, using the same Zeeman-splitting technique that revealed an average value of $B = 6\,\mu$G in the neutral interstellar gas of our Galaxy[4]. This is unexpected, as the leading theory of magnetic field generation, the mean-field dynamo model, predicts large-scale magnetic fields to be weaker in the past rather than stronger[5].

We detected Zeeman splitting of the $z = 0.692$, 21-cm absorption line in the direction of the quasar 3C 286 (refs 6, 7) using the 100-m Robert C. Byrd Green Bank Telescope (GBT) of the National Radio Astronomy Observatory. The absorption arises in a damped Lyman α (Lyα) system (henceforth denoted DLA-3C286) that is drawn from a population of neutral gas layers widely thought to be the progenitors of modern galaxies[8]. The radio data for DLA-3C286 are summarized in Fig. 1, which shows the line-depth spectra constructed from the measurable quantities used to describe polarized radiation, that is, the Stokes parameters. We show line-depth spectra constructed from the $I(v)$ and $V(v)$ Stokes parameters (where v denotes frequency) near the 839.4-MHz frequency centroid of the redshifted 21-cm absorption line. Figure 1a shows the line-depth spectrum constructed from $I(v)$. A Gaussian fit to the absorption line in Fig. 1a yields a redshift of $z = 0.6921526 \pm 0.0000008$, a central optical depth of $\tau_0 = 0.095 \pm 0.006$, and a velocity dispersion of $\sigma_v = 3.75 \pm 0.20\,\mathrm{km\,s^{-1}}$, which are in good agreement with previous results[6,7].

In Fig. 1b, we plot the line-depth spectrum constructed from $V(v)$, which shows the classic 'S curve' pattern expected for Zeeman splitting. From our least-squares fit to the data, we find that $B_{\rm los} = 83.9 \pm 8.8\,\mu$G, where $B_{\rm los}$ is the magnetic field component projected along the line of sight (we note that the direction of $B_{\rm los}$ is unknown because the instrumental sense of circular polarization was not calibrated). This magnetic field differs in two respects from the magnetic fields obtained from Zeeman splitting arising in interstellar clouds in the Galaxy. First, the field strength corresponds to the line-of-sight component of the mean field $\langle B_{\rm los}\rangle$ averaged over transverse dimensions exceeding 200 pc, as very-long-baseline interferometry observations of the 21-cm absorption line show that the gas layer must extend across more than 0.03″ to explain the difference between the velocity centroids of the fringe amplitude and phase-shift spectra[9] (although the data are consistent with a magnetic field coherence length of less than 200 pc, the resulting gradient in magnetic pressure would produce velocity differences exceeding the shift of $\sim 3\,\mathrm{km\,s^{-1}}$ across 200 pc detected by very-long-baseline interferometry). By contrast, the transverse dimensions of radio beams subtended at neutral interstellar clouds in the Galaxy are typically less than 1 pc. Second, this field is at least an order of magnitude stronger than the 6-μG average of magnetic fields inferred from Zeeman splitting for such clouds[4].

We obtained further information about conditions in the absorbing gas in DLA-3C286 from accurate optical spectra acquired with the HIRES echelle spectrograph on the Keck I 10-m telescope. Figure 2 shows velocity profiles for several resonance absorption lines arising from dominant low-ionization states of abundant elements. The results of our least-squares fit of Voigt profiles to the data are shown in Table 1, where the optical redshift is displaced $+3.8 \pm 0.2\,\mathrm{km\,s^{-1}}$ from the 21-cm redshift. This solution also yields ionic column densities from which we derived the logarithmic metal abundances with respect to solar abundances, [M/H], and dust-to-gas ratios with respect to the Galactic interstellar medium, [D/G]. These are among the lowest values of [M/H] and [D/G] deduced for damped Lyα systems at $z = 0.7$ (refs 10, 11). The low metallicity indicates a history of low star formation rates. Because the intensity of far-ultraviolet radiation emitted by young massive stars is proportional to the concurrent star formation rate per unit area, $\Sigma_{\rm SFR}$, low values of $\Sigma_{\rm SFR}$ should result in low grain photoelectric heating rates per hydrogen atom, $\Gamma_{\rm pe}$ (ref. 11). This is consistent with the low upper limit, $\Gamma_{\rm pe} < 10^{-27.4}\,\mathrm{erg\,s^{-1}}$ per hydrogen atom, obtained by combining the assumption of thermal balance with the absence of C II* absorption (that is, absorption from C II in the excited $^2P_{3/2}$ fine-structure state) at a wavelength of 1,335.7 Å in the previous low-resolution Hubble Space Telescope spectra of quasar 3C 286 (ref. 12), and indicates that $\Sigma_{\rm SFR} < 10^{-2.9} M_\odot\,\mathrm{yr^{-1}\,kpc^{-2}}$ (95% confidence level), which is less than the solar-neighbourhood value of $10^{-2.4} M_\odot\,\mathrm{yr^{-1}\,kpc^{-2}}$ (ref. 13).

As a result, we have detected an unusually strong magnetic field at $z = 0.692$ with a coherence length that probably exceeds 200 pc in neutral gas that is quiescent, metal poor, nearly dust free, and presents little evidence of star formation. To model this configuration, we first consider the magnetostatic equilibrium of a plane-parallel sheet with in-plane magnetic field $B_{\rm plane}$ orthogonal to the vertical gravitational field exerted by gas with perpendicular mass surface density Σ. In magnetostatic equilibrium, the total mid-plane pressure, $B^2_{\rm plane}/8\pi + \rho\sigma_v^2$, equals the 'weight' of the gas, $\pi G\Sigma^2/2$, where ρ is the mass volume density of the gas and G is the gravitational constant. However, because the pressure-to-weight ratio exceeds

[1]Department of Physics and Center for Astrophysics and Space Sciences, University of California, San Diego, La Jolla, California 92093-0424, USA. [2]Astronomy Department, University of California, Berkeley, California 94720-3411, USA. [3]UCO-Lick Observatory; University of California, Santa Cruz, Santa Cruz, California 95464, USA.

715 in DLA-3C286, the magnetized gas cannot be confined by its self-gravity. Therefore, self-consistent magnetostatic configurations are ruled out unless the contribution of stars to Σ exceeds $\sim 350 M_{\odot}\ \mathrm{pc}^{-2}$. Although this is larger than the $50 M_{\odot}\ \mathrm{pc}^{-2}$ surface density perpendicular to the solar neighbourhood, such surface densities are common in the central regions of galaxies. In fact, high surface densities of stars probably confine the highly magnetized gas in the nuclear rings of barred spirals. These exhibit total field strengths of $\sim 100\ \mu$G, inferred by assuming equipartition of magnetic and cosmic-ray energy densities[1]. However, because the rings are associated with regions of active star formation, high molecular content and high dust content, they are unlikely sites for the magnetic field detected in DLA-3C286.

On the other hand, the absorption site might consist of highly magnetized gas confined by the gravity exerted by a disk of old stars. The H I disks found at the centres of early-type S0 and elliptical galaxies[14] are possible prototypes. Support for this idea stems from a high-resolution image obtained with the Hubble Space Telescope: a Wide Field and Planetary Camera 2 (WFPC2) I-band image, from which the quasar has been subtracted, reveals residual emission spread over angular scales of $\sim 1''$ (ref. 15). The asymmetry of the light distribution with respect to the point-source quasar suggests

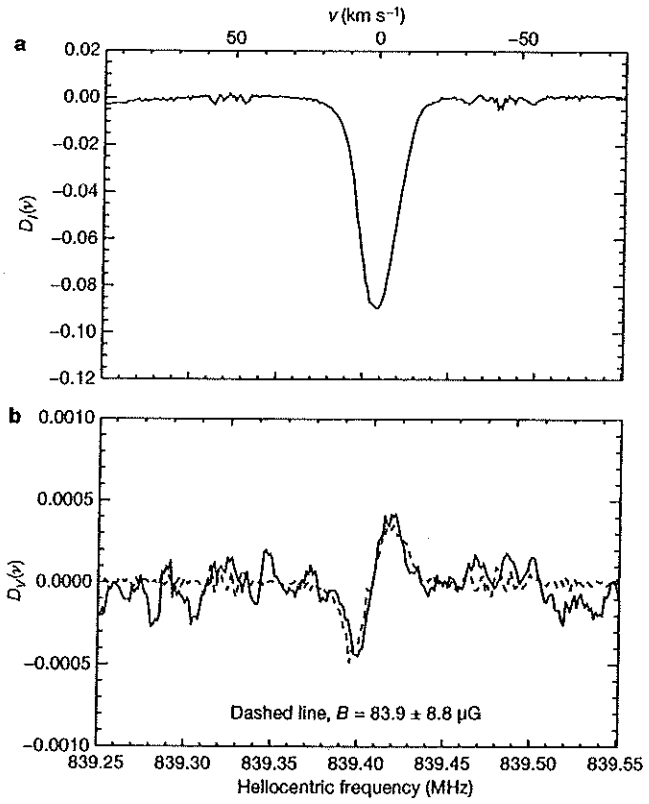

Figure 1 | Line-depth spectra of Stokes parameters. Data acquired in 12.6 hours of on-source integration with the GBT radio antenna. Because the GBT feeds detect only orthogonal, linearly polarized signals, whereas Zeeman splitting requires measuring circular polarization to construct $V(v)$, we generated $V(v)$ by cross-correlation techniques[23]. The velocity $v = 0\ \mathrm{km\ s^{-1}}$ corresponds to $z = 0.6921526$. **a**, Line-depth function $D_I(v) \equiv (I(v) - I_c(v))/I_c(v)$. Here $I(v) \equiv s_0 + s_{90}$, with s_θ the power measured in linear-polarization position angle θ, corresponds to the total intensity spectrum, and $I_c(v)$ is a model fit to the $I(v)$ continuum. $D_I(v) = \exp(-\tau(v)) - 1$, where $\tau(v) \equiv (\tau(v)_0 + \tau(v)_{90})/2$ is the average optical depth in the two orthogonal states of linear polarization[4]. **b**, Line-depth function $D_V(v) \equiv V(v)/I_c(v)$, where $V(v) \equiv s_{\mathrm{RCP}} - s_{\mathrm{LCP}}$ is the difference in power between the right-hand and left-hand circularly polarized (respectively RCP and LCP) signals. Here $D_V(v) = -(\tau_V(v)/2)\exp(-\tau(v))$, where $\tau_V(v) \equiv \tau_{\mathrm{RCP}}(v) - \tau_{\mathrm{LCP}}(v) \ll 1$ (ref. 4) is the difference between the optical depths of RCP and LCP photons. For Zeeman splitting of the 21-cm line, the degeneracy of the $F = 0$ to $F = 1$ hyperfine transition is removed because the $m_F = -1, 0, +1$ states differ in energy. This results in a small frequency difference between absorbed LCP photons ($m_F = -1$) and RCP photons ($m_F = +1$). $V(v)$ is crucial for detecting Zeeman splitting because the orthogonal, circularly polarized states of the photon are eigenstates of the spin angular momentum operator with eigenvalues $\pm\hbar$, that is, angular momenta directed along or opposite to the direction of photon propagation[24]. When $B_{\mathrm{los}} = B$, transitions between the hyperfine $F = 0$ and $F = 1$ states occur exclusively through absorption of LCP or RCP photons through excitation of the $m_F = -1$ and $m_F = +1$ hyperfine states, respectively. Because $V(v)$ is the difference in the RCP and LCP intensities, the resulting $V(v)$ line profile is the difference between two Gaussian absorption profiles with frequency centroids shifted by $\Delta\nu_B = 2.8 B_{\mathrm{los}}(1+z)^{-1}$ Hz (where B_{los} is measured in microgauss). The 'S curve' pattern is due to the sign flip in RCP-minus-LCP intensity difference as v passes through the line centre.

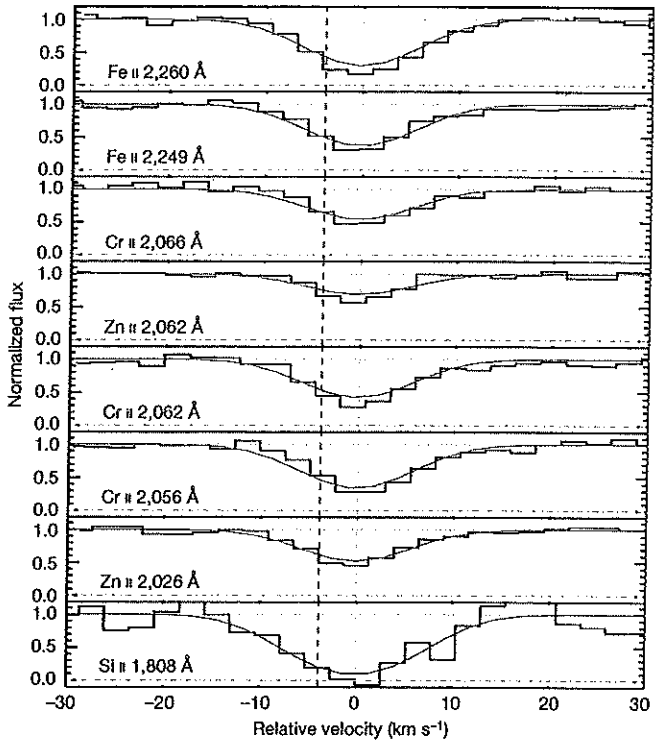

Figure 2 | HIRES velocity profiles for dominant low-ionization states of abundant elements in the 21-cm absorber in the direction of quasar 3C 286. Spectral resolution is $\Delta v = 7.0\ \mathrm{km\ s^{-1}}$ and the average signal-to-noise ratio per 2.1-km-s^{-1} pixel is about 30:1. The bold dashed vertical line denotes the velocity centroid of the single-dish 21-cm absorption feature and the faint dashed vertical lines denotes the velocity centroid of the resonance line shown in the figure. Our least-squares fit of Voigt profiles (red) to the data (black) yields ionic column densities as well as the redshift centroid and velocity dispersion shown in Table 1 (lower and upper green horizontal lines refer to zero and unit normalized fluxes, respectively). Because refractory elements such as Fe and Cr can be depleted onto dust grains[25], we used the volatile elements Si and Zn to derive a logarithmic metal abundance with respect to solar abundances of [M/H] = −1.30. The depletion ratios [Fe/Si] and [Cr/Zn] were then used to derive a conservative upper limit on the logarithmic dust-to-gas ratio relative to Galactic values of [D/G] < −1.8.

On the other hand, the absorption site might consist of highly magnetized gas confined by the gravity exerted by a disk of old stars. The H I disks found at the centres of early-type S0 and elliptical galaxies[14] are possible prototypes. Support for this idea stems from a high-resolution image obtained with the Hubble Space Telescope: a Wide Field and Planetary Camera 2 (WFPC2) I-band image, from which the quasar has been subtracted, reveals residual emission spread over angular scales of $\sim 1''$ (ref. 15). The asymmetry of the light distribution with respect to the point-source quasar suggests

Table 1 | Physical parameters of DLA-3C286 inferred from optical absorption

Ion, X	$\log_{10}[N(\mathrm{X})\ (\mathrm{cm}^{-2})]$	[X/H]
H I	21.25 ± 0.02	—
Fe II	15.09 ± 0.01	−1.66 ± 0.02
Cr II	13.44 ± 0.01	−1.48 ± 0.02
Zn II	12.53 ± 0.03	−1.39 ± 0.03
Si II	>15.48	>−1.31

Redshift, $z = 0.69217485 \pm 0.00000058$; velocity dispersion, $\sigma_v = 3.08 \pm 0.13\ \mathrm{km\ s^{-1}}$. N(X), column density of ion X.

Spin-orbit Energy splitting corresponds to $\Delta E = \hbar\Omega$, $\propto \vec{L}\cdot\vec{S}$
where Ω is the frequency at which the electron spin precesses around the orbital angular momentum vector

Gyroscope Precession (A Classical Interlude)

$$\text{Torque} = \vec{r} \times \vec{F}_g = \frac{d\vec{L}}{dt} = I\frac{d\vec{\omega}}{dt}$$

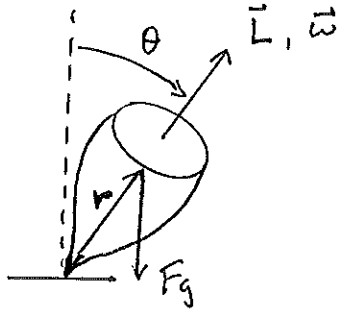

$\vec{L} = I\vec{\omega}$

Torque is into the page.

Looking down the dashed line:

$$d\omega = \omega \sin\theta \, d\phi$$

$$\frac{d\omega}{dt} = \omega \sin\theta \frac{d\phi}{dt}$$

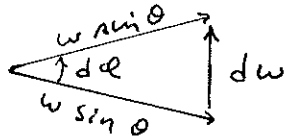

Let $\frac{d\phi}{dt} = \Omega$ the precession angular velocity

So $I\frac{d\omega}{dt} = I\omega\sin\theta\,\Omega$

$$\boxed{\frac{d\vec{L}}{dt} = \vec{\Omega} \times \vec{L}}$$

$$\text{Torque} = \vec{\Omega} \times \vec{L}$$

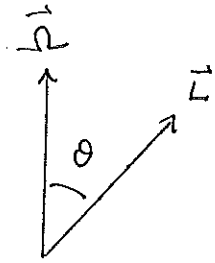

Magnetic Dipole Precession (classical)

In the presence of an external magnetic field, a magnetic dipole experiences a torque

$$\text{Torque} = \vec{\mu} \times \vec{B}$$

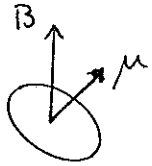

which causes it to precess with angular velocity Ω given by

$$\vec{\mu} \times \vec{B} = \vec{\Omega} \times \vec{L}$$

$$\vec{\mu} = -\frac{e}{2mc}\vec{L}$$

or $\Omega = \frac{\mu B}{L}$ But the energy splitting due to quantized values of L is $\Delta E = -\vec{\mu}\cdot\vec{B}$

So $\Omega = \frac{\Delta E}{L\cos\theta} = \frac{\Delta E}{L_z}$ $\boxed{\Delta E = \Omega m_\ell \hbar}$ where $\Omega = \frac{eB}{2mc}$

Zeeman effect = anomalous, when $S \neq 0$

Usually an even number of states is observed. This is due to electron spin, where $L_S = \sqrt{S(S+1)}\,\hbar$, $S = \frac{1}{2}$

$L_{S,z} = m_S \hbar$, $m_S = \pm\frac{1}{2}$

It is found that $\mu_S = 2.00232\,\mu_B$ where $\mu_B = \frac{e\hbar}{2mc}$ "Bohr magneton"

So $\mu_S = -\frac{e\hbar}{mc} m_S$

The total magnetic moment is $\vec{\mu} = \sum_i \left[\frac{1}{2}\frac{e}{mc}\vec{l}_i + \frac{e}{mc}\vec{l}_{S,i}\right]$

That is, $\vec{\mu}$ is the vector sum of all of the orbital and spin magnetic moments of the electrons.

Since $\vec{L} = \sum_i \vec{l}_i$ and $\vec{S} = \sum_i \vec{l}_{S,i}$, we have

$$\vec{\mu} = -\frac{1}{2}\left(\frac{e}{mc}\right)(\vec{L} + 2\vec{S}) = -\frac{1}{2}\left(\frac{e}{mc}\right)(\vec{J} + \vec{S})$$

Note that the net magnetic moment $\vec{\mu}$ is not necessarily parallel to the total angular momentum $\vec{J}$.

If there were no external B field, $\vec{L}$, $\vec{S}$, and $\vec{\mu}$ would precess about $\vec{J}$ with frequency proportional to the energy shift in L-S coupling, which is proportional to $\vec{L}\cdot\vec{S}$, while $\vec{J}$ would remain fixed.

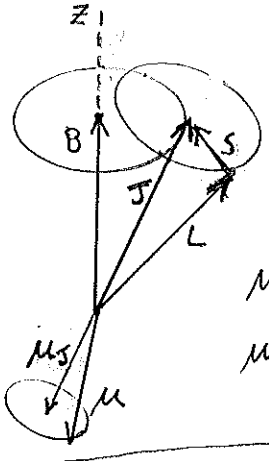

$$\mu_x = \mu_J \frac{\vec{S}\cdot\vec{B}}{|J||B|}$$

$$\mu_J = \frac{\vec{\mu}\cdot\vec{J}}{|J|}$$

$$\langle \mu_z \rangle = \frac{\vec{\mu}\cdot\vec{J}}{|J|}\,\frac{\vec{J}\cdot\vec{B}}{|J||B|}$$

When an external field is applied, $\vec{J}$ will precess about $\vec{B}$. If the field is weak, this precession frequency will be much lower than the precession frequency of $\vec{L}$ and $\vec{S}$ around $\vec{J}$. So the time averaged component of μ along B, or $\langle \mu_z \rangle$, will be approximately the component of μ along J times the component of J along B.

$$\text{So } \Delta E = -\vec{\mu}\cdot\vec{B} = \frac{1}{2}\frac{e}{mc}(\vec{J}+\vec{S})\cdot\frac{\vec{J}}{|J|^2}(\vec{J}\cdot\vec{B})$$

$$= \frac{1}{2}\frac{e}{mc}\left(\frac{|J|^2+\vec{J}\cdot\vec{S}}{|J|^2}\right)J_z B$$

but $\vec{J}\cdot\vec{S} = \frac{1}{2}(|J|^2+|S|^2-|L|^2)$

[Because $(\vec{J}-\vec{S})\cdot(\vec{J}-\vec{S}) = |J|^2+|S|^2-2\vec{J}\cdot\vec{S} = L^2$]

$$\text{So } \Delta E = \frac{1}{2}\frac{eB}{mc}\left[\frac{|J^2|+\frac{1}{2}(|J|^2+|S|^2-|L|^2)}{|J|^2}\right]J_z$$

But $J_z = M_J\hbar$

and $|J|^2 = J(J+1)$
$|S|^2 = S(S+1)$
$|L|^2 = L(L+1)$

$$\text{So } \Delta E = \frac{1}{2}\frac{e\hbar}{mc}B\,g\,M_J$$

where $$g = 1+\frac{J(J+1)+S(S+1)-L(L+1)}{2J(J+1)}$$

is the Landé g factor

The Zeeman effect removes the degeneracy with respect to M_J.

Consider a transition between two levels, 1 and 2

$$\Delta E_1 = \frac{1}{2}\frac{e\hbar}{mc}B\,g_1 M_{J_1} \qquad \Delta E_2 = \frac{1}{2}\frac{e\hbar}{mc}B\,g_2 M_{J_2}$$

Then $$\Delta E_{12} = \frac{1}{2}\frac{e\hbar}{mc}B\,(g_1 M_{J_1} - g_2 M_{J_2})$$

If $g_1 = g_2$, then there will be three components to the line because of the selection rules that $\Delta M_J = 0, \pm 1$. But in general, g_1 does not have to be equal to g_2.

Paschen-Back effect

Zeeman effect for strong magnetic field, when the magnetic splitting becomes greater than the fine-structure splitting. is analogous to the normal Zeeman effect

$$\Delta E = \frac{e\hbar}{2mc}(m_\ell + 2m_s)B \qquad \text{to first approximation}$$

Allowed transitions have $\Delta m_\ell = 0, \pm 1$, $\Delta m_s = 0$. $\vec{L}$ and $\vec{S}$ are no longer coupled, and since $\Delta S = 0$, the spin can be ignored. In the context of the Figure on page 186, μ_z becomes simply $\vec{\mu}_L \cdot \vec{B}$ in the limit of large B, when $\vec{J}$ precesses around $\vec{B}$ much faster than $\vec{L}$ and $\vec{S}$ precess around $\vec{J}$. For optical lines, the transition to the Paschen-Back regime occurs around $B \approx 10^5$ G.

Quadratic Zeeman effect

For $B > 10^6$ G, the term in the Hamiltonian proportional to the square of the external electromagnetic field (which was previously ignored) begins to be important, and becomes dominant for $B > 10^7$ G. The quadratic term is positive, and causes a decrease in wavelength (blue shift) of all three Zeeman components.

$$H = \frac{1}{2m}\left(\tilde{p} - \frac{e\tilde{A}}{c}\right)^2 - \frac{e}{mc}\tilde{S}\cdot\tilde{B} - \frac{e^2}{r} \qquad \vec{A} = \frac{1}{2}\vec{r}\times\vec{B}$$

$$H_m = \frac{eB}{2mc}(\tilde{\ell}_z + 2\tilde{s}_z) + \frac{e^2B^2}{8mc^2}r^2\sin^2\theta$$

The quadratic term in the Zeeman shift for hydrogen

$$\Delta\lambda_Q\,(\text{Å}) = -4.98\times10^{-23}\lambda_0^2\,(n^4 - n'^4)(1+m^2)B^2$$

where n = upper level
n' = lower level
$m = 0, \pm 1$ for π and σ transitions, respectively.